Article published online: 2022-05-19

Original article

Quantitative Assessment of Radionuclide Uptake and Positron Emission Tomography-computed Tomography Image Contrast

Hasford Francis[1,2,3], John Humphrey Amuasi[1], Kyere Augustine Kwame[1], Mboyo Di Tamba Vangu[3]

[1]Department of Medical Physics, School of Nuclear and Allied Sciences, University of Ghana, [2]Medical Radiation Physics Centre, Radiological and Medical Sciences Research Institute, Ghana Atomic Energy Commission, Accra, Ghana, [3]Department of Nuclear Medicine, Charlotte Maxeke Johannesburg Academic Hospital, University of the Witwatersrand, Johannesburg, South Africa

Abstract

Radionuclide uptake and contrast for positron emission tomography-computed tomography (PET-CT) images have been assessed in this study using NEMA image quality phantom filled with background activity concentration of 5.3 kBq/mL fluorodeoxyglucose (F-18 FDG). Spheres in the phantom were filled in turns with water to mimic cold lesions and FDG of higher activity concentrations to mimic tumor sites. Transaxial image slices were acquired on the PET-CT system and used for the evaluation of mean standard uptake value (SUV_{mean}) and contrasts for varying sphere sizes at different activity concentrations of 10.6 kBq/mL, 21.2 kBq/mL, and 42.4 kBq/mL. For spheres of same sizes, SUV_{mean} increased with increase in activity concentration. SUV_{mean} was increased by 80.6%, 83.5%, 63.2%, 87.4%, and 63.2% when activity concentrations of spheres with a diameter of 1.3 cm, 1.7 cm, 2.2 cm, 2.8 cm, and 3.7 cm, respectively, were increased from 10.6 kBq/mL to 42.4 kBq/mL. Average percentage contrast between cold spheres (cold lesions) and background activity concentration was estimated to be 89.96% for the spheres. Average contrast for the spheres containing 10.6 kBq/mL, 21.2 kBq/mL, and 42.4 kBq/mL were found to be 110.92%, 134.48%, and 150.52%, respectively. The average background contrast variability was estimated to be 2.97% at 95% confidence interval ($P < 0.05$).

Keywords: Hot lesion, image contrast, image quality phantom, radionuclide activity

Introduction

Imaging of tumors with integrated positron emission tomography-computed tomography (PET-CT) system has become a standard component of diagnosis, staging and therapy response evaluation in oncology.[1-5] The use of fluorine fluorodeoxyglucose (F-18 FDG) for oncology imaging accounts for the majority of all PET-CT imaging procedures since the increased accumulation of FDG relative to normal tissue is a useful marker for many cancers.[6] Several methods exist for measuring the rate and/or total amount of FDG accumulation in tumors. PET scanners are designed to measure *in vivo* radioactivity concentration (kBq/mL), which is directly linked to the FDG concentration. Typically, however, it is the relative

Address for correspondence:
Mr. Hasford Francis,
Medical Radiation Physics Centre, Radiological and Medical Sciences Research Institute, Ghana Atomic Energy Commission,
PO Box LG 80, Legon, Accra, Ghana.
E-mail: haspee@yahoo.co.uk

Access this article online

Quick Response Code:

Website: www.wjnm.org

DOI: 10.4103/1450-1147.174702

This is an open access article distributed under the terms of the Creative Commons Attribution-NonCommercial-ShareAlike 3.0 License, which allows others to remix, tweak, and build upon the work non-commercially, as long as the author is credited and the new creations are licensed under the identical terms.

For reprints contact: reprints@medknow.com

How to cite this article: Francis H, Amuasi JH, Kwame KA, Vangu MD. Quantitative assessment of radionuclide uptake and positron emission tomography-computed tomography image contrast. World J Nucl Med 2016;15:167-72.

tissue uptake of FDG that is of interest. The two most significant sources of variation that occur in practice are the amount of injected FDG and the patient size.[7]

The practice of using standard uptake value (SUV) thresholds for diagnosis is known to be affected by a number of factors, which does not make it wholistically acceptable worldwide. These factors have been discussed extensively by a number of researchers.[1,4,8-15] Two common reasons for the inconsistent use of SUVs in practice are: (i) Accurate staging and diagnostic information do not have to depend upon accurate image quantification, since the relative image content or appearance is often sufficient for such purposes,[16] and (ii) measured SUVs have large degree of variability due to physical and biological sources of error, as well as inconsistent and non-optimized image acquisition, processing and analysis.[1,17-21] However, the use of SUV as a measurement of relative tissue/organ uptake facilitates comparisons between patients, and has been suggested as a basis for diagnosis.[7,22,23] Standard uptake value, which is a simplified measure of radionuclide uptake, is until date thought to be the most widely used method for the quantification of F-18 FDG PET studies, although other methods have been developed as well.[24,25]

Tomographic image quality of PET-CT images is determined by a number of different performance parameters, primarily the contrast and spatial resolution, scanner sensitivity, tomographic uniformity, and the process that is used to reconstruct the images.[26] Due to the complexity of variation in uptake of radiopharmaceuticals and the large range of patient sizes and shapes, the characteristics of radioactivity distributions often vary greatly and a single study with a phantom cannot simulate all clinical imaging conditions. However, such studies give some indications of image quality for a particular imaging situation that could be reproduced on different scanners at different times. The study of image quality (contrast) follows closely the NEMA NU2-2007 recommendations.[27] Image contrast is assessed to produce images simulating those obtained in a total body imaging study involving both hot and cold lesions. Radioactivity is present outside the PET scanner to mimic out-of-field radioactivity, and spheres of different diameters are imaged in a simulated body phantom with nonuniform attenuation. Image quality is assessed by calculating image contrast and background variability ratios for both hot and cold spheres.

Materials and Methods

Image quality phantom (IEC/NEMA 2001 body phantom, Middleton, Wisconsin, USA)[28] was used for the study. The phantom container was filled with 5.3 kBq/mL F-18 FDG to serve as background activity. This activity concentration is an approximation of the typical background uptake observed on clinical data and hence, is recommended for the use of NEMA phantom devices.[26,29]

Step 1

Five spheres in the phantom (with diameters 1.3 cm, 1.7 cm, 2.2 cm, 2.8 cm, and 3.7 cm) were filled with tap water to mimic cold lesion imaging. The phantom was set up and aligned in a supine position on PET-CT system (Biograph 40, Siemens, Memphis, Tennessee, USA) for imaging as shown in Figure 1a. PET-CT images of the phantom were acquired in 3 min (one bed position) and displayed in 512 × 512 matrix. Transaxial image slice centering on the spheres as shown in Figure 1b was selected for the analysis.

Step 2

The spheres were emptied and refilled with F-18 FDG of concentration 10.6 kBq/mL such that the ratio of concentration between spheres and background was 2:1. Images were acquired in the same setup and acquisition conditions as in step 1.

Step 3–4

The procedure was repeated for activity concentrations of 21.2 kBq/mL and 42.4 kBq/mL such that the ratios of concentration between sphere and background were 4:1 and 8:1, respectively. Figure 1c indicates hot spots from the higher activity concentration in spheres.

Standard uptake values (SUVs) and image contrasts (Q) for the different activity concentrations in the spheres were assessed by drawing regions of interest (ROIs) over the respective target areas, and employing equations 1–4. Four transaxial image slices (one from each of the four steps) centering on all spheres were used for the analysis.

$$SUV = \frac{Activity\ Concentration\ in\ ROI\ (kBq\ /\ mL)}{Injected\ Activity\ (MBq)\ /\ Body\ Weight\ (kg)} \quad (1)$$

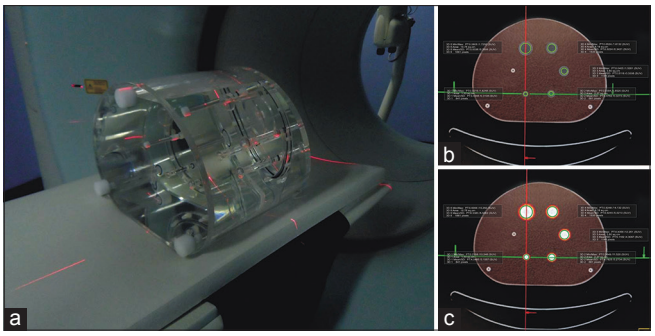

Figure 1: (a) NEMA image quality phantom under scanning (b) PET-CT image showing cold spheres (lesions) (c) PET-CT image showing hot spheres (lesions)

Percentage contrasts for hot and cold spheres were estimated by equations (2) and (3), respectively.[26]

$$Q_H = 100\left[\frac{(C_H - C_B)/C_B}{(a_H - a_B)/a_B}\right] \quad (2)$$

$$Q_C = 100\left[\frac{C_B - C_C}{C_B}\right] \quad (3)$$

where C_H denotes the counts of activity in ROI for hot sphere and C_B denotes average counts of activity in corresponding background ROIs; a_H is activity concentration in the hot sphere and a_B is activity concentration in the background; C_C denotes the counts of activity in ROI for cold sphere.

Percentage background contrast variability (N) was estimated from equation 4.[26]

$$N = 100 \times \frac{\sqrt{\frac{1}{K-1}\sum_{k=1}^{K}(C_{B,k} - C_B)^2}}{C_B} \quad (4)$$

where K is the number of background ROIs (i.e. 48).

Results

The study was performed to assess the quality of PET-CT images by simulating those obtained in total body imaging involving hot and cold lesions. Four transaxial image slices corresponding to cold sphere (water) and hot spheres (10.6 kBq/mL, 21.2 kBq/mL, and 42.4 kBq/mL) were used in examining the trends of radionuclide uptake and image contrasts in the study. SUV, which indirectly characterizes the level of radionuclide uptake in tissues, was used as a measure to analyze the quantities of radionuclide activity in spheres of different sizes in the image quality phantom. The image quality phantom mimics a human being with varying tumor sites and sizes. For uniform activity distribution with no excretion, SUV = 1 assuming tissue density of 1 g/cm^3. Mean SUV (SUV_{mean}) was used as quantity for measurement in this study because its value does not change significantly with image reconstruction factors such as matrix size, number of subsets, and iterations, compared to maximum SUV (SUV_{max}).[30]

Uptake values (SUV_{mean}) for the different activity concentrations and respective sphere sizes are presented in Table 1 and graphically shown in Figure 2. Pixel intensity plot from image J, along the central point of a hot spot in the transaxial images is indicated in Figure 3. The percentage contrast estimates are presented in Table 2. Variation of percentage contrast with the sphere's activity concentrations is presented in Figure 4 while the variation of percentage contrast with spherical sizes is presented in Figure 5. The background contrast variability estimates for different ROI sizes are presented in Table 3 and graphically presented in Figure 6.

Discussion

For spheres of same sizes, SUV_{mean} increased with increase in activity concentration [Figure 2]. Between 10.6 kBq/mL and 42.4 kBq/mL F-18 FDG solution, SUV_{mean} increased by 80.6%, 83.5%, 63.2%, 87.4%, and 63.2% for spheres of diameters 1.3 cm, 1.7 cm, 2.2 cm, 2.8 cm, and 3.7 cm, respectively. Radionuclide uptake values correspond proportionally to the concentration of activity in organs or tissues; hence, higher concentration is associated with higher SUV_{mean} as established in this study. For any particular activity concentration, the differences in SUV_{mean} among the different spherical sizes were relatively minimal. Activity concentrations of 10.6 kBq/mL, 21.2 kBq/mL, and 42.4 kBq/mL produced deviations of 19.4%, 13.4%, and 11.4%, respectively,

Table 1: Standard uptake values (mean) for ROIs of different activity concentrations

Activity concentration in sphere	ROI† diameter (cm)	Area of ROI (cm^3)	No. of pixels	SUV_{min}‡ (g/mL)	SUV_{max}§ (g/mL)	SUV_{mean}•±SD (g/mL)
10.6 kBq/ml	1.3	1.33	841	0.42	7.33	3.46±1.03
FDG	1.7	2.27	881	0.79	8.07	3.51±1.24
	2.2	3.80	1146	0.28	8.84	3.75±0.97
	2.8	6.16	1535	0.56	9.62	3.64±1.28
	3.7	10.75	1861	0.20	10.16	4.13±1.31
21.2 kBq/mL	1.3	1.33	841	0.48	8.99	4.86±0.72
FDG	1.7	2.27	881	0.21	9.60	5.37±1.20
	2.2	3.80	1146	0.31	10.39	5.19±1.02
	2.8	6.16	1535	0.33	11.11	5.51±1.33
	3.7	10.75	1861	0.35	12.83	5.29±1.18
42.4 kBq/mL	1.3	1.33	841	0.22	10.25	6.25±1.56
FDG	1.7	2.27	881	0.38	11.52	6.44±1.14
	2.2	3.80	1146	0.41	12.26	6.12±1.66
	2.8	6.16	1535	0.52	14.13	6.82±1.01
	3.7	10.75	1861	1.61	15.25	6.74±1.76

†ROI: Region of interest; ‡SUV_{min}: Minimum standard uptake value; §SUV_{max}: Maximum standard uptake value; •SUV_{mean}: Mean standard uptake value

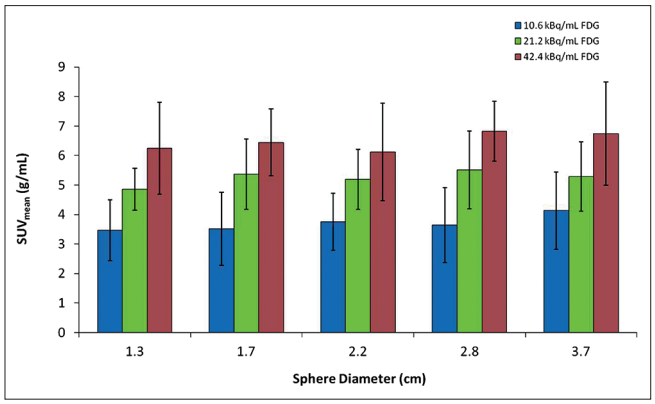

Figure 2: Mean standard uptake values for ROIs of different activity concentrations

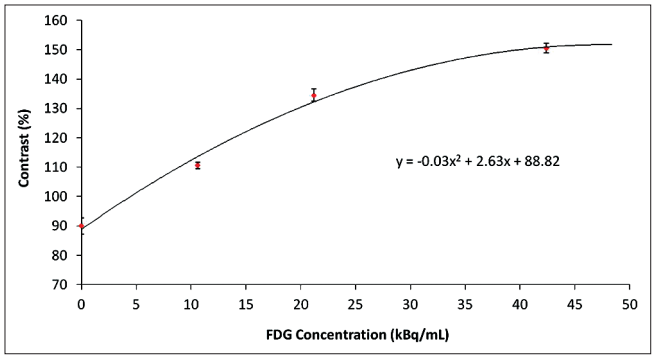

Figure 4: Percentage contrast variability with activity concentration in sphere

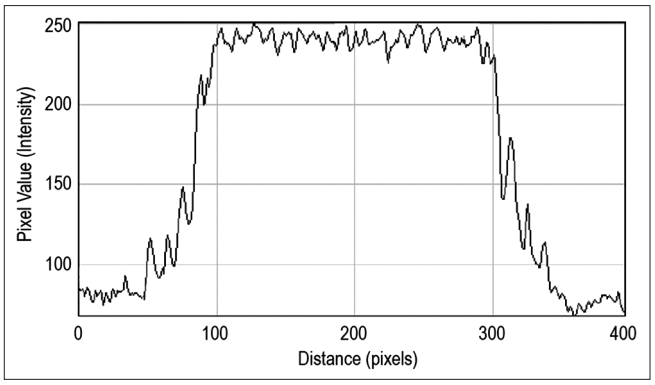

Figure 3: Pixel intensities along line of interest for hot spot

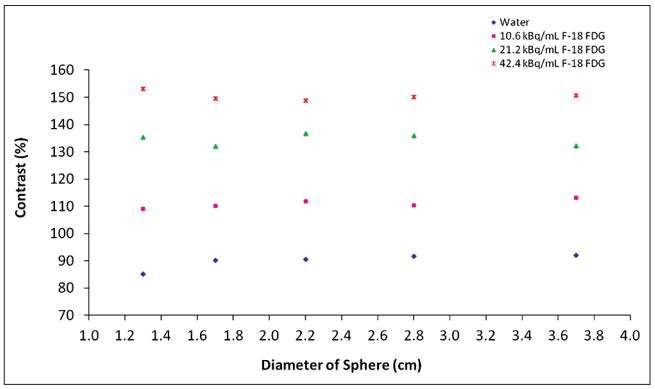

Figure 5: Percentage contrast for spheres of different sizes and activities

between the highest and least recorded SUV_{mean}. Table 1 presents detailed SUV data for the study.

From Figure 3, in the region around the central point in the hot spot, pixels have intensities of approximately 250 units, and background activity has pixel intensities of less than 100 units. Image pixel intensities have a linear relation with activity concentration; hence, the uneven nature at the peak of the curve implies imperfect uniformity of activity distribution in the sphere. Deviations of pixel values at the peak of the pixel plots for hot spots in the study were all within 10%, signifying a relatively uniform concentration.

Image contrast evaluation between hot or cold spots (lesions) and background radionuclide activity in acquired images reveal to some extent the level of image quality produced on PET-CT systems. Figures 4 and 5 show the percentage contrast variabilities with the sphere's activity concentrations and sizes, respectively [Table 2]. Percentage contrast for the cold spots ranged from 85.2% to 92% for the different sized water-filled spheres, with mean contrast estimated to be 89.96 ± 2.76%. Average contrast for the spheres containing 10.6 kBq/mL, 21.2 kBq/mL, and 42.4 kBq/mL were found to be 110.92 ± 1.60%, 134.48 ± 2.15%, and 150.52 ± 1.58%, respectively, in

Table 2: Percentage contrast estimates

ROI diameter	Contrast (%)			
	Water	10.6 kBq/mL	21.2 kBq/mL	42.4 kBq/mL
1.3 cm	85.19	109.09	135.4	153.09
1.7 cm	90.28	110.16	132.02	149.72
2.2 cm	90.63	111.82	136.65	148.89
2.8 cm	91.68	110.34	136	150.22
3.7 cm	92	113.19	132.34	150.68
Average	89.96±2.76	110.57±1.09	134.48±2.15	150.52±1.58

ROI: Region of interest

reference to the background activity. From the smallest to the biggest sphere, percentage contrast fairly remained constant in the case of water and the three activity concentrations, implying that tumor size may not directly have a significant influence on image contrast at constant activity concentration. By doubling the concentration from 10.6 kBq/mL to 21.2 kBq/mL, the contrast increased by 21% while doubling from 21.4 kBq/mL to 42.4 kBq/mL resulted in 12% increase in contrast. The contrast curve in Figure 4 is projected to assume a plateau shape beyond 42.4 kBq/mL where the radionuclide activity concentration ratio between sphere and background is 8:1.

For spheres of diameter 1.3 cm, 1.7 cm, 2.2 cm, 2.8 cm, and 3.7 cm, contrast increased by 79.7%, 65.8%, 64.3%,

Table 3: Background variability estimates

	ROI‡ diameter				
	1.3 cm	1.7 cm	2.2 cm	2.8 cm	3.7 cm
Number of ROIs	48	48	48	48	48
P value	0.028	0.027	0.028	0.028	0.028
Mean background counts (cts)	2427	4362	6831	11566	17232±490
Standard error (RMSE†)	72	134	199	356	490
Counts (at 95% confidence interval)	2427±141	4362±263	6831±390	11566±698	17232±960
Background contrast variability (%)	2.96	3.07	2.91	3.08	2.85
Average BCV⁂ (%)			2.97±0.1		

‡ROI: Region of interest; †RMSE: Root-mean-square error; ⁂BCV: Background contrast variability

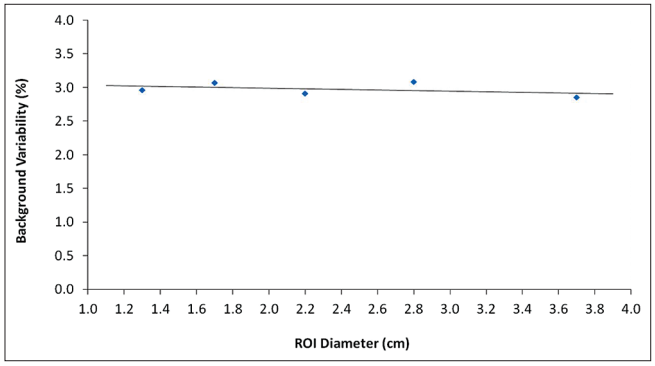

Figure 6: Variability of contrast in background activity

63.9%, and 63.8% between a cold lesion (water) of no radionuclide activity and a hot lesion of 42.4 kBq/mL, as depicted in Figure 5. By increasing the activity concentration, bigger sized spheres recorded relatively less increase in contrast compared to smaller spheres. This observation could be a result of the count density being high for smaller volumes compared to larger volumes. At constant activity concentration, contrast remains relatively the same for hot spheres of different sizes, an indication that tumors of different sizes but containing similar activity concentrations may likely record similar contrast values.

Background contrast variability (N) estimation allows assessment of the accuracy of absolute quantification of radioactivity concentration in the uniform volume of interest inside the phantom. Contrast within the background activity distribution varied by approximately 3% as shown in Figure 6. Using ROIs of different sizes (1.3 cm, 1.7 cm, 2.2 cm, 2.8 cm, and 3.7 cm), the average background contrast variability was estimated to be 2.97 ± 0.1% (2.85–3.08%) at 95% confidence interval with $P < 0.05$ [Table 3]. The tolerance level of ±5% relative to baseline estimates for contrast and background variability recommended by the IAEA Human Health Series 1[26] could not be assessed due to unavailable baseline data.

Conclusion

The study has analyzed SUVs and contrast of PET-CT images with the use of NEMA image quality phantom. For same sized spheres, SUV_{mean} increases with increase in activity concentration, affirming that radionuclide uptake values correspond proportionally to the concentration of activity in organs or tissues. Radionuclide activity concentration was also shown to have linear relation with image pixel intensities. Contrast between tumor sites (hot lesions) and background activity distribution increases with increasing activity concentration in the tumor but the contrast is likely to plateau beyond certain concentration ratios between the tumor and background activity. At constant activity concentration, contrast remains relatively the same for tumors (hot lesions) of different sizes. Background contrast variability has also been determined to be approximately 3%, indicating a very good uniformity within the background activity concentration.

Acknowledgement

This research serves as a part of the Doctor of Philosophy (Ph.D.) study of Francis Hasford. The author acknowledges with thanks the support of the International Atomic Energy Agency, Ghana Atomic Energy Commission, University of Ghana, and the Nuclear Medicine Department of CM Johannesburg Academic Hospital/University of Witwatersrand.

Financial support and sponsorship

Nil.

Conflicts of interest

There are no conflicts of intrest.

References

1. Weber WA. Use of PET for monitoring cancer therapy and for predicting outcome. J Nucl Med 2005;46:983-95.
2. Weber WA, Grosu AL, Czernin J. Technology insight: Advances in molecular imaging and an appraisal of PET/CT scanning. Nat Clin Pract Oncol 2008;5:160-70.
3. De Geus-Oei LF, van der Heijden HF, Corstens FH, Oyen WJ. Predictive and prognostic value of FDG-PET in nonsmall-cell lung cancer: A systematic review. Cancer 2007;110:1654-64.
4. Fletcher JW, Djulbegovic B, Soares HP, Siegel BA, Lowe VJ, Lyman GH, *et al*. Recommendations on the use of 18F-FDG PET in oncology. J Nucl Med 2008;49:480-508.

5. Bastiaannet E, Groen H, Jager PL, Cobben DC, van der Graaf WT, Vaalburg W, *et al*. The value of FDG-PET in the detection, grading and response to therapy of soft tissue and bone sarcomas; a systematic review and meta-analysis. Cancer Treat Res 2004;30:83-101.
6. Kelloff GJ, Hoffman JM, Johnson B, Scher HI, Siegel BA, Cheng EY, *et al*. Progress and promise of FDG-PET imaging for cancer patient management and oncologic drug development. Clin Cancer Res 2005;11:2785-808.
7. Kinahan PE, Fletcher JW. Positron emission tomography-computed tomography standardized uptake values in clinical practice and assessing response to therapy. Semin Ultrasound CT MR 2010;31:496-505.
8. Keyes JW Jr. SUV: Standard uptake or silly useless value? J Nucl Med 1995;36:1836-9.
9. Young H, Baum R, Cremerius U, Herholz K, Hoekstra O, Lammertsma AA, *et al*. Measurement of clinical and subclinical tumour response using [18F]-fluorodeoxyglucose and positron emission tomography: Review and 1999 EORTC recommendations. European Organization for Research and Treatment of Cancer (EORTC) PET Study Group. Eur J Cancer 1999;35:1773-82.
10. Delbeke D, Coleman RE, Guiberteau MJ, Brown ML, Royal HD, Siegel BA, *et al*. Procedure guideline for tumor imaging with 18F-FDG PET/CT 1.0. J Nucl Med 2006;47:885-95.
11. Cheson BD, Pfistner B, Juweid ME, Gascoyne RD, Specht L, Horning SJ, *et al*. Revised response criteria for malignant lymphoma. J Clin Oncol 2007;25:579-86.
12. Coleman RE, Delbeke D, Guiberteau MJ, Conti PS, Royal HD, Weinreb JC, *et al*.; American College of Radiology; Society of Nuclear Medicine; Society of Computed Body Tomography and Magnetic Resonance. Concurrent PET/CT with an integrated imaging system: Intersociety dialogue from the joint working group of the American College of Radiology, the Society of Nuclear Medicine, and the Society of Computed Body Tomography and Magnetic Resonance. J Nucl Med 2005;46:1225-39.
13. Juweid ME, Stroobants S, Hoekstra OS, Mottaghy FM, Dietlein M, Guermazi A, *et al*.; Imaging Subcommittee of International Harmonization Project in Lymphoma. Use of positron emission tomography for response assessment of lymphoma: Consensus of the Imaging Subcommittee of International Harmonization Project in Lymphoma. J Clin Oncol 2007;25:571-8.
14. Shankar LK, Hoffman JM, Bacharach S, Graham MM, Karp J, Lammertsma AA, *et al*.; National Cancer Institute. Consensus recommendations for the use of 18F-FDG PET as an indicator of therapeutic response in patients in National Cancer Institute trials. J Nucl Med 2006;47:1059-66.
15. Bourguet P, Blanc-Vincent MP, Boneu A, Bosquet L, Chauffert B, Corone C, *et al*. Summary of the standards, options and recommendations for the use of positron emission tomography with 2-[18F] fluoro-2-deoxy-D-glucose (FDG-PET scanning) in oncology (2002). Br J Cancer 2003;89(Suppl 1):S84-91.
16. Coleman RE. Is quantitation necessary for oncological PET studies? For. Eur J Nucl Med Mol Imaging 2002;29:133-5.
17. Boellaard R, Krak NC, Hoekstra OS, Lammertsma AA. Effects of noise, image resolution, and ROI definition on the accuracy of standard uptake values: A simulation study. J Nucl Med 2004;45:1519-27.
18. Stahl A, Ott K, Schwaiger M, Weber WA. Comparison of different SUV-based methods for monitoring cytotoxic therapy with FDG PET. Eur J Nucl Med Mol Imaging 2004;31:1471-8.
19. Lowe VJ, DeLong DM, Hoffman JM, Coleman RE. Optimum scanning protocol for FDG-PET evaluation of pulmonary malignancy. J Nucl Med 1995;36:883-7.
20. Soret M, Bacharach SL, Buvat I. Partial-volume effect in PET tumor imaging. J Nucl Med 2007;48:932-45.
21. Jaskowiak CJ, Bianco JA, Perlman SB, Fine JP. Influence of reconstruction iterations on 18F-FDG PET/CT standardized uptake values. J Nucl Med 2005;46:424-8.
22. Boellaard R. Standards for PET image acquisition and quantitative data analysis. J Nucl Med 2009;50(Suppl 1):11-20S.
23. Gambhir SS. Molecular imaging of cancer with positron emission tomography. Nat Rev Cancer 2002;2:683-93.
24. Graham MM, Peterson LM, Hayward RM. Comparison of simplified quantitative analyses of FDG uptake. Nucl Med Biol 2000;27:647-55.
25. Sadato N, Tsuchida T, Nakamura S, Waki A, Uematsu H, Takahashi N, *et al*. Non-invasive estimation of the net influx constant using the standardized uptake value for quantification of FDG uptake of tumours. Eur J Nucl Med 1998;25:559-64.
26. International Atomic Energy Agency. Quality Assurance for PET and PET-CT Systems: Human Health Series No. 1. Vienna, Austria: International Atomic Energy Agency (IAEA); 2009. p. 61-7.
27. National Electrical Manufacturers Association. Performance Measurements of Positron Emission Tomographs, NEMA Standard NU2-2007. Washington, DC: National Electrical Manufacturers Association (NEMA); 2007. p. 25-33.
28. International Electrotechnical Commission. Radionuclide Imaging Devices-Characteristics and Test Conditions-Part 1: Positron Emission Tomographs, IEC 61675-1. Geneva: International Electrotechnical Commission (IEC); 2008. p. 1-4.
29. Discovery™ PET-CT 690 NEMA Test Procedures. GE Healthcare 2008. Waukesha: p. 5-40.
30. International Atomic Energy Agency. PET-CT Atlas on Quality Control and Image Artefacts. Human Health Series No. 27. Vienna, Austria: International Atomic Energy Agency (IAEA) 2014. p. 11-2.